



# The integrated stress response suppresses antiviral RNA interference by autophagy-mediated degradation of the **RNA-induced silencing complex**

Qiyu Wang<sup>a</sup>, Lingyue Chen<sup>a</sup>, Jiayin Wang<sup>a</sup> (b, Zhijian Chen<sup>a</sup>, Zixian Ma<sup>a</sup>, Xuan Xie<sup>a</sup>, Xiaohui Zeng<sup>a</sup>, Yuanyuan Bie<sup>a</sup>, and Zhaowei Wang<sup>a,1</sup> (b

Affiliations are included on p. 12.

Edited by Shou-Wei Ding, University of California Riverside College of Natural and Agricultural Sciences, Riverside, CA; received May 12, 2025; accepted September 8, 2025 by Editorial Board Member Peter Palese

The small interfering RNA (siRNA) pathway is a highly conserved antiviral defense mechanism in vertebrates and invertebrates. Although the core components of this pathway are well characterized, its upstream regulatory networks remain poorly understood. Here, we identify the integrated stress response (ISR) as a negative regulator of the siRNA pathway, and demonstrate that the picorna-like virus CrPV (Cricket Paralysis Virus) exploits this mechanism for immune evasion. Mechanistically, the picorna-like virus triggers the ISR through transcriptional suppression of ppp1r15, a key regulator of eukaryotic initiation factor  $2\alpha$  (eIF2 $\alpha$ ) dephosphorylation. ISR activation subsequently induces the autophagy-lysosomal pathway by up-regulating Atg1 transcription in an ATF4-dependent manner. This process leads to selective degradation of Argonaute 2 (Ago2) and other core components of the RNA-induced silencing complex (RISC), thereby suppressing the host RNA interference (RNAi) machinery and enhancing viral replication. Our findings uncover an unconventional immune evasion strategy employed by a picorna-like virus and establish a previously unrecognized crosstalk between the ISR and siRNA pathways.

integrated stress response | RNA interference | autophagy | picorna-like virus

Innate immunity serves as the first line of defense against microbial invasion (1–3). In insects, innate immunity relies on conserved innate immunity signaling pathways, such as Toll, Immune Deficiency (IMD), and siRNA, to detect and defend against pathogens. Initial research in insects identified the evolutionarily conserved Toll and IMD pathways as key mechanisms for combating bacterial and fungal infections. These pathways regulate NF-κB family transcription factors to induce antimicrobial peptide (AMP) production (4–6). Specifically, the Toll pathway, activated by fungi and Gram-positive bacteria, utilizes the NF-κB factors Dorsal/Dif to induce AMPs like Drosomycin (Drs). Conversely, the IMD pathway primarily responds to Gram-negative bacteria and employs the NF-κB homolog Relish to regulate AMPs such as Diptericin (Dpt). Subsequent studies further demonstrate that both pathways participate in defending against specific viral infections (7–10). The siRNA pathway, initially identified as a major antiviral pathway in plants, plays a critical role as a potent antiviral defense system in insects and also in mammals (11–20). This pathway is initiated by the recognition of double-stranded RNA (dsRNA) segments derived from viral replicative intermediates. The dsRNA is processed by Dicer, a dsRNA-specific endoribonuclease, which cleaves dsRNA into 21- to 23-nucleotide siRNAs. Subsequently, these virus-derived siRNAs are transferred by the Dicer-R2D2 complex to Argonaute to form RISC, which guides the specific pairing and destruction of homologous viral RNA in infected cells (21–23).

The fruit fly *Drosophila melanogaster*, like other insects, lacks acquired immune responses and relies primarily on innate immunity mechanisms, including the siRNA pathway, to defend against viruses (11–14). For instance, *Drosophila* mutants lacking *Dicer-2* (*Dcr-2*), which encodes the sole siRNA-producing Dicer protein in *Drosophila*, exhibit increased susceptibility to viruses such as Flock House Virus (FHV), Drosophila C virus (DCV), and Sindbis virus (SINV) (12). Similarly, Drosophila mutants with Argonaute 2 (Ago2) deficiency show heightened susceptibility and mortality upon infection with DCV and Cricket Paralysis Virus (CrPV) (24). Intriguingly, emerging evidence suggests that core components of the siRNA pathway play multifaceted roles in modulating diverse immune signaling cascades. In a seminal study, Deddouche et al. demonstrated that Dcr-2 mediates the induction of the antiviral protein Vago, which subsequently regulates DCV infection (25). On the other hand, our previous work revealed that Dcr-2 positively regulates Toll

# **Significance**

RNA interference (RNAi) and integrated stress response (ISR) are evolutionarily conserved pathways that can respond to viral infection in both vertebrates and invertebrates. However, the potential crosstalk between these two pathways remains poorly understood. Our study reveals that an insect picorna-like virus activates the ISR, which in turn leads to the autophagy-mediated degradation of the RNA-induced silencing complex (RISC), the core effector complex of RNAi. This process suppresses the antiviral RNAi response and enhances viral replication. Our results provide a striking example of a virus co-opting a host pathway, distinct from directly encoding viral suppressors of RNAi (VSRs), to evade RNAi. Furthermore, we elucidate the molecular mechanisms underlying the ISR-autophagy-RNAi regulatory axis, which may be conserved across diverse animal species.

Author contributions: Q.W. and Z.W. designed research; Q.W., L.C., J.W., Z.C., Z.M., X.X., X.Z., Y.B., and Z.W. performed research; Q.W. and Z.W. analyzed data; and Q.W. and Z.W. wrote the paper.

The authors declare no competing interest.

This article is a PNAS Direct Submission. S.D. is a guest editor invited by the Editorial Board.

Copyright © 2025 the Author(s). Published by PNAS. This article is distributed under Creative Commons Attribution-NonCommercial-NoDerivatives License 4.0 (CC BY-NC-ND).

<sup>1</sup>To whom correspondence may be addressed. Email: wangzhw29@mail.sysu.edu.cn.

This article contains supporting information online at https://www.pnas.org/lookup/suppl/doi:10.1073/pnas. 2511857122/-/DCSupplemental.

Published October 8, 2025.

protein expression at the posttranscriptional level, thereby facilitating the activation of Toll immune signaling (26). Despite these significant advances in understanding the downstream immunological functions of the siRNA pathway, the upstream regulatory mechanisms governing its activity remain poorly understood.

The ISR is a highly conserved cellular signaling pathway among eukaryotic cells that is activated in response to various stress conditions. A central event in ISR is the phosphorylation of eukaryotic initiation factor  $2\alpha$  (eIF2 $\alpha$ ), mediated by one of four eIF2 $\alpha$ kinases: protein kinase R (PKR), PKR-like endoplasmic reticulum kinase (PERK), general control nonderepressible 2 (GCN2), and heme-regulated eIF2α kinase (HRI) (27). This phosphorylation event globally attenuates protein synthesis while selectively enhancing the translation of specific genes, such as activating transcription factor 4 (ATF4). The ISR also plays a pivotal role in antiviral innate immunity (28). For example, PKR is activated mainly by dsRNA during the infection of various viruses, thereby blocking the translation of viral mRNAs (29-31). The PERK-ATF4 axis of ISR can suppress the replication of transmissible gastroenteritis virus (TGEV) by inducing interferon-I (IFN-I) and inhibiting viral protein synthesis (32). Additionally, GCN2 recognizes integrase from HIV type 1 (HIV-1) and restricts both viral integration (33) and viral RNA translation (34). However, the role of the ISR in antiviral response in invertebrates remains largely unexplored.

Here, we demonstrate that CrPV infection suppresses the transcription of *protein phosphatase 1 regulatory subunit 15 (ppp1r15)*, thereby triggering ISR activation. Moreover, ISR activation

enhances *Autophagy-related 1* (*Atg1*) transcription through the phospho-eIF2α-ATF4 axis, and the up-regulation of *Atg1* is sufficient to promote the degradation of Ago2 via the autophagy-lysosomal pathway. Furthermore, CrPV also promotes the degradation of other RISC proteins, including FMR1, RM62, and VIG, via a similar mechanism. This process results in the suppression of RNAi and facilitates viral immune evasion. Our findings elucidate a previously unrecognized crosstalk between the ISR and RNAi pathways, and reveal an upstream regulatory mechanism for the RNAi pathway. Given the evolutionary conservation of both the RNAi and ISR pathways in invertebrates and vertebrates, these findings provide insights into the innate immunity network and highlight potential targets for antiviral therapeutic development.

## **Results**

**CrPV Infection Induces the ISR.** Previous studies have established that diverse mammalian viruses can activate the ISR in their host cells (29–34). Building upon this foundation, we aimed to determine whether insect viruses similarly induce ISR activation. To this end, we infected *Drosophila* S2 cells with four distinct RNA viruses: FHV, DCV, CrPV, and *Drosophila* X virus (DXV), and assessed the levels of phosphorylated eIF2 $\alpha$  (P-eIF2 $\alpha$ ), a classic molecular marker of ISR activation. Consistent with a previous study (35), our results revealed that infection with CrPV, a picorna-like virus, led to a significant up-regulation of P-eIF2 $\alpha$  (Fig. 1*A*; quantified in Fig. 1*B*). The specificity of the

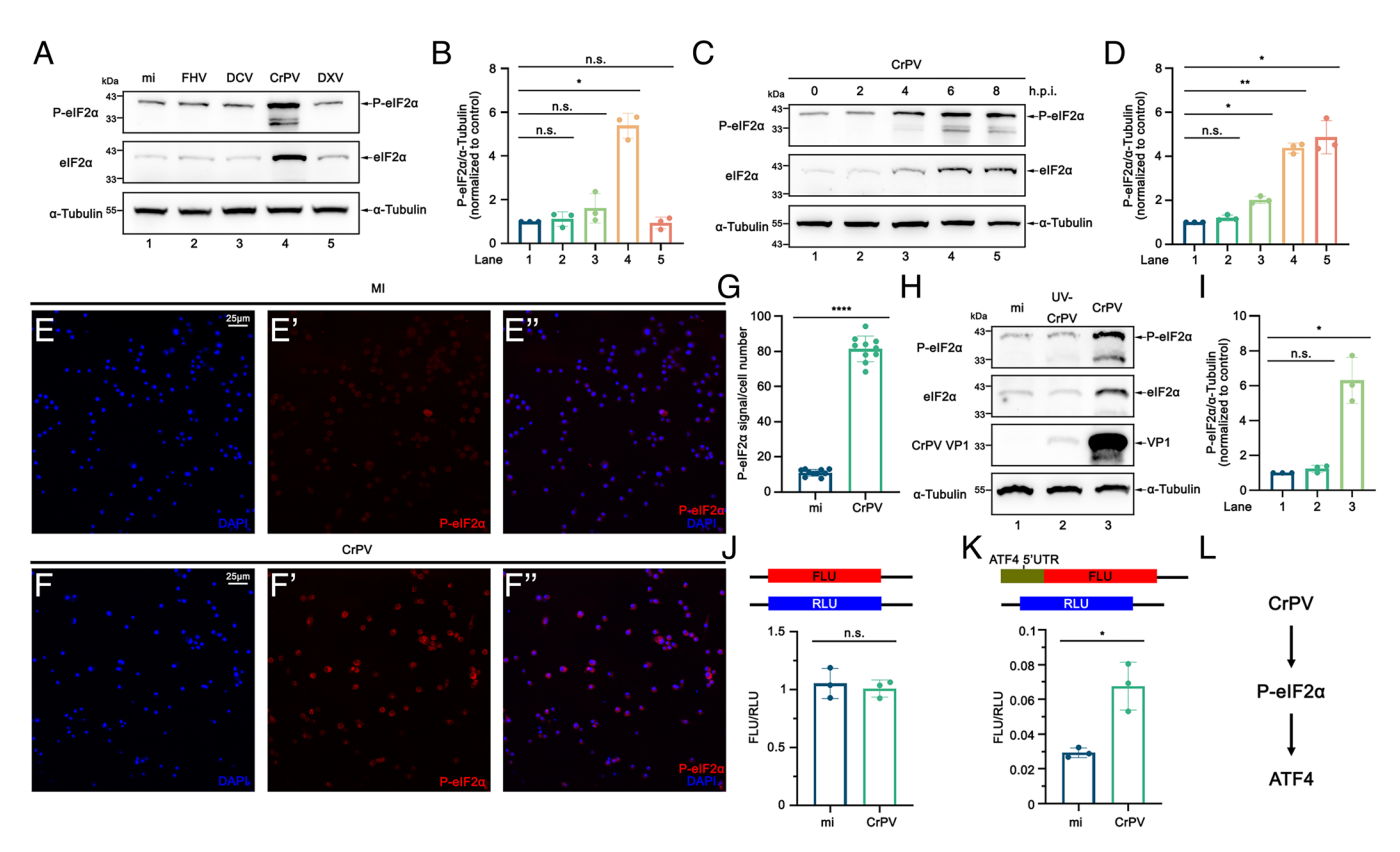


**Fig. 1.** CrPV infection induces the ISR. (*A*) Cultured S2 cells were mock infected or infected with FHV (MOI = 1), DCV (MOI = 1), CrPV (MOI = 1), or DXV (MOI = 1) for 12 h and subjected to western blot analysis using indicated antibodies. (*B*) Quantification of relative P-eIF2 $\alpha$  levels in (*A*) from three independent experiments. (*C*) Cultured S2 cells were infected with CrPV (MOI = 1) for 0, 2, 4, 6, or 8 h and then subjected to western blot analysis using indicated antibodies. (*D*) Quantification of relative P-eIF2 $\alpha$  levels in (*C*) from three independent experiments. (*E* and *F*) Cultured S2 cells were mock infected (*E*) or infected with CrPV (MOI = 1) (*F*) for 8 h and stained with DAPI (*E* and *F*) and anti-P-eIF2 $\alpha$  antibody (*E*' and *F*'). Merged images are shown in *E*" and *F*". (*G*) The relative P-eIF2 $\alpha$  signal in (*E* and *F*) (n = 10). (*H*) Cultured S2 cells were infected with CrPV (MOI = 1) or UV-inactivated CrPV for 8 h and subjected to western blot analysis using indicated antibodies. (*I*) Quantification of relative P-eIF2 $\alpha$  levels in (*H*) from three independent experiments. (*J* and *K*) Cultured S2 cells were transfected with the indicated reporter constructs. The FLU/RLU ratio was measured from the dual-luciferase assay (n = 3). (*L*) Schematic diagram of CrPV infection induces the ISR.

anti-P-eIF2 $\!\alpha$  and anti-total eIF2 $\!\alpha$  antibodies were confirmed in SI Appendix, Fig. S1. In contrast, other viruses failed to elicit this response. Moreover, we found that the P-eIF2 $\alpha$  level was significantly elevated as early as 4 h post CrPV infection and continued to rise in correspondence with the duration of infection thereafter (Fig. 1C; quantified in Fig. 1D). This finding was further corroborated by immunofluorescence analysis, which revealed a marked increase in eIF2α phosphorylation in CrPV infected cells compared to mock infected controls (Fig. 1 E and F; quantified in Fig. 1*G*).

Surprisingly, we observed an up-regulation of total eIF2α protein levels during CrPV infection (Fig. 1 A and C, quantified in SI Appendix, Fig. S2 A and B). To investigate the molecular mechanisms underlying this phenomenon, we examined both  $eIF2\alpha$ mRNA level and protein stability in the context of CrPV infection. Under CrPV infection, we observed a statistically nonsignificant decrease in eIF2\alpha mRNA levels (>50\% reduction in average at 4 h post CrPV infection; *SI Appendix*, Fig. S3A). Conversely, CrPV infection significantly enhanced eIF2α protein stability, extending its half-life from 3-4 h (mock infection) to >5 h (SI Appendix, Fig. S3 B and C; quantified in SI Appendix, Fig. S3D). Notably, this stabilization was absent in the nonphosphorylatable eIF2 $\alpha$  mutant (eIF2 $\alpha$ <sup>S51A</sup>) (*SI Appendix*, Fig. S3 *E* and *F*; quantified in SI Appendix, Fig. S3G), indicating that CrPV may specifically stabilize phosphorylated eIF2 $\alpha$ .

We subsequently sought to elucidate whether the increase in eIF2α phosphorylation is dependent on CrPV replication. To this end, we infected S2 cells with UV-inactivated CrPV and normal CrPV. As expected, CrPV loses its replicative capacity upon UV treatment (Fig. 1H). Our result revealed that UV-inactivated CrPV markedly diminished the up-regulation of P-eIF2 $\alpha$  (Fig. 1H; quantified in Fig. 11 and SI Appendix, Fig. S2C), indicating that CrPV replication is required for the up-regulation of P-eIF2 $\alpha$ . To further characterize ISR activation, we monitored the translational regulation of ATF4, a key downstream transcription factor in the ISR pathway, using a dual-luciferase reporter assay. Our data showed that CrPV infection also significantly enhanced ATF4 translation (Fig. 1 J and K) without altering ATF4 transcription (SI Appendix, Fig. S4A). Altogether, our findings demonstrated that CrPV infection enhances the phosphorylation and protein stability of eIF2 $\alpha$ , as well as the translation of ATF4, indicating that CrPV can induce the ISR (Fig. 1*L*).

CrPV Induces the ISR by Inhibiting ppp1r15 Transcription. Given the absence of PKR and HRI in *Drosophila*, phosphorylation of eIF2 $\alpha$  relies on the kinases PERK and GCN2. To identify which kinase is responsible for eIF2α phosphorylation during CrPV infection, we respectively knocked down PERK and GCN2 using RNAi in cultured S2 cells. In agreement with previous findings (36), knockdown of either PERK or GCN2 did not mitigate the up-regulation of P-eIF2α during CrPV infection (Fig. 2 A and C; quantified in Fig. 2 B and D; knockdown efficiency validated in SI Appendix, Fig. S5 A and B). Nevertheless, simultaneous knockdown of both kinases effectively suppressed CrPV-induced phosphorylation of eIF2α (SI Appendix, Fig. S6A; quantified in SI Appendix, Fig. S6B; knockdown efficiency validated in SI Appendix, Fig. S6 C and D) and further suppressed CrPVinduced translation of ATF4 (SI Appendix, Fig. S6E, knockdown efficiency validated in SI Appendix, Fig. S6 F and G), indicating that the presence of either PERK or GCN2 is sufficient to mediate CrPV-induced ISR. Considering that PERK and GCN2 respond to distinct stress signals, this observation led us to investigate alternative regulatory mechanisms. A previous study reported that the phosphorylation of eIF2α can be regulated by

GADD34, a regulatory subunit of PP1, in a dephosphorylation process that forms a negative feedback loop in mammals (37). Based on this study, we proposed that CrPV may promote the phosphorylation of eIF2α by inhibiting ppp1r15, the Drosophila homolog of mammalian GADD34. To validate this hypothesis, we first examined whether down-regulation of ppp1r15 is sufficient to induce the phosphorylation of eIF2 $\alpha$  in *Drosophila*. As we expected, knocking down *ppp1r15* promoted eIF2α phosphorylation in S2 cells (Fig. 2E; quantified in Fig. 2 F and G; knockdown efficiency validated in SI Appendix, Fig. S5C), larval fat bodies (Fig. 2 H and I) and wing discs (Fig. 2 J and K). We next attempted to determine whether CrPV inhibits ppp1r15. Our data demonstrated that CrPV infection significantly reduced the transcription of ppp1r15 at 2 h post infection (h.p.i.) (Fig. 2L). This decrease was dependent on viral replication, as UV-inactivated CrPV did not elicit a reduction in ppp1r15 transcription (Fig. 2M). In contrast, FHV, DCV, or DXV infection failed to suppress *ppp1r15* transcription (SI Appendix, Fig. S7 A-C), explaining why only CrPV specifically induces eIF2 $\alpha$  phosphorylation (Fig. 1A; quantified in Fig. 1B). Moreover, we observed that knockdown of ppp1r15 blocked the further up-regulation of P-eIF2α during CrPV infection (Fig. 2N; quantified in Fig. 2 O and P; knockdown efficiency validated in *SI Appendix*, Fig. S5*D*), indicating that the reduction of ppp1r15 is responsible for eIF2α phosphorylation during CrPV infection. Additionally, we found that knockdown of ppp1r15 led to a significant up-regulation of total eIF2 $\alpha$  (Fig. 2 E and N, quantified in Fig. 2 G and P), which is similar to that observed during CrPV infection, indicating that the reduction of ppp1r15 also contributes to the up-regulation of total eIF2α during CrPV infection. In summary, our findings demonstrated that CrPV induces the ISR by inhibiting *ppp1r15* transcription, rather than by activating PERK or GCN2 (Fig. 2Q).

The ISR Promotes Ago2 Protein Degradation to Suppress the siRNA Pathway. We next sought to elucidate how the ISR might influence CrPV in turn. We found that knockdown of ATF4 significantly reduced CrPV genomic RNA level (Fig. 3A; knockdown efficiency validated in SI Appendix, Fig. S8A) and viral titer (Fig. 3B; knockdown efficiency validated in SI Appendix, Fig. S8B). Similarly, simultaneous knockdown of PERK and GCN2 significantly inhibited CrPV replication (SI Appendix, Fig. S9A; knockdown efficiency validated in SI Appendix, Fig. S9 B and C), indicating that activation of the ISR benefits CrPV replication. We next examined whether other RNA viruses gain an advantage upon ISR activation. Our data showed that ISR activation induced by ppp1r15 knockdown enhanced DCV replication (SI Appendix, Fig. S10C; knockdown efficiency validated in SI Appendix, Fig. S10D) but had no effect on FHV (SI Appendix, Fig. S10A; knockdown efficiency validated in SI Appendix, Fig. S10B) and only a mild (not statistically significant) effect on DXV (SI Appendix, Fig. S10E; knockdown efficiency validated in SI Appendix, Fig. S10F). Previous studies have demonstrated that ATF4 is able to promote the transcription of thor, the Drosophila homolog of mammalian 4E-BP, thereby enhancing internal ribosome entry site (IRES)-dependent translation (38, 39). Considering that CrPV RNA contains a 5'-IRES and an intergenic region (IGR)-IRES, which are essential for the translation of viral polyprotein 1 and 2 respectively (40-42), the ISR may up-regulate thor transcription, and thus promoting viral protein translation and viral replication (35). Indeed, knockdown of ppp1r15 significantly up-regulated thor mRNA in S2 cells (SI Appendix, Fig. S11A; knockdown efficiency validated in SI Appendix, Fig. S11B). However, we found that CrPV infection dramatically decreased the mRNA level of thor (SI Appendix, Fig. S11C). Additionally, neither the 5'-IRES nor the

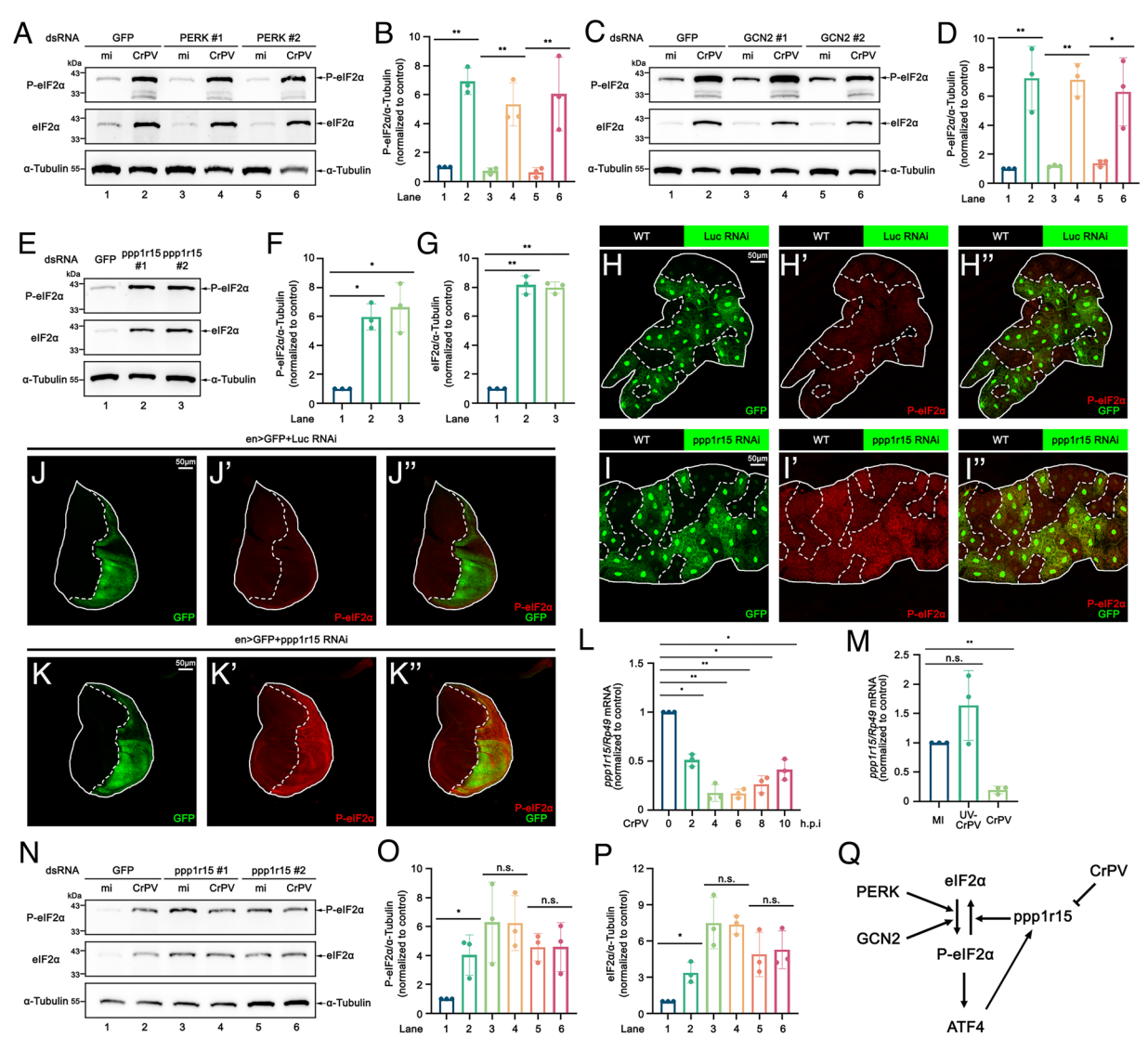


**Fig. 2.** CrPV infection induces the ISR by inhibiting ppp1r15 transcription. (A) Cultured S2 cells were transfected with dsRNAs against the indicated genes and then mock infected or infected with CrPV (MOI = 1) for 12 h. Cell lysates were subsequently subjected to western blot analysis using indicated antibodies. (B) Quantification of relative P-eIF2α levels in (A) from three independent experiments. (C) Cultured S2 cells were transfected with dsRNAs against the indicated genes and then mock infected or infected with CrPV (MOI = 1) for 12 h. Cell lysates were subsequently subjected to western blot analysis using indicated antibodies. (D) Quantification of relative P-eIF2α levels in (C) from three independent experiments. (E) Cultured S2 cells were transfected with dsRNAs against the indicated genes and subjected to western blot analysis using indicated antibodies. (F and G) Quantification of relative P-eIF2α (F) or total eIF2α (G) levels in (E) from three independent experiments. (H and I) Fat bodies bearing GFP-labeled clones of indicated genotypes stained with anti-P-eIF2α antibody (H' and I'). Merged images are shown in H'' and I''. (J and K) Wing discs from flies of indicated genotypes stained with anti-P-eIF2α antibody (J' and K'). Merged images are shown in J'' and K''. (L) Cultured S2 cells were infected with CrPV (MOI = 1) for 0, 2, 4, 6, 8, or 10 h and then analyzed by RT-qPCR to quantify ppp1r15 mRNA levels. (M) Cultured S2 cells were infected with CrPV (MOI = 1) or UV-inactivated CrPV for 8 h and analyzed by RT-qPCR to quantify ppp1r15 mRNA levels. (N) Cultured S2 cells were transfected with dsRNAs against the indicated genes and then mock infected or infected with CrPV (MOI = 1) for 12 h. Cell lysates were subsequently subjected to western blot analysis using indicated antibodies. (O and P) Quantification of relative P-eIF2α (O) or total eIF2α (P) levels in (N) from three independent experiments. (Q) Schematic diagram of CrPV infection induces the ISR by inhibiting ppp1r15 transcription.

IGR-IRES of CrPV exhibited a significant increase in translation efficiency in the context of CrPV infection (*SI Appendix*, Fig. S11 *D* and *E*). These findings revealed that the effect of the ISR on CrPV replication is not contingent upon the promotion of *thor*-dependent viral protein translation (*SI Appendix*, Fig. S11*F*).

Given previous studies showing that phosphorylation of eIF2 $\alpha$  is involved in the antiviral NF- $\kappa$ B immune pathway (32, 43), we further investigated whether the ISR promotes viral replication by limiting antiviral immune responses. We knocked down ATF4 and examined the Toll and IMD pathways, two antiviral NF- $\kappa$ B pathways in Drosophila (7–10), as well as the JAK-STAT pathway, which is also an important antiviral immune pathway in Drosophila (44) and closely related to the IMD pathway (45). Our data showed that inhibiting ISR through ATF4 knockdown significantly up-regulated  $Turandot\ M\ (TotM)$  and  $Cecropin\ B\ (CecB)$ ,

the downstream genes of the JAK-STAT and IMD pathway respectively, but not other downstream genes of JAK-STAT, Toll, and IMD pathways in the absence of CrPV (SI Appendix, Fig. S12 A–F, knockdown efficiency validated in SI Appendix, Fig. S12G). In the context of CrPV infection, only Dpt, a downstream gene specific for the IMD pathway, was significantly up-regulated following ATF4 knockdown (SI Appendix, Fig. S12 A–F). We further examined whether JAK-STAT, Toll, and IMD pathways play antiviral roles in Drosophila S2 cells. We found that knockdown of classical components of JAK-STAT, Toll, and IMD pathways did not affect CrPV replication (SI Appendix, Fig. S13A, knockdown efficiency validated in SI Appendix, Fig. S13 B–G). These observations indicated that the ISR may contribute to the inhibition of the JAK-STAT and/or IMD pathway, however, this mechanism is not sufficient to promote viral replication.

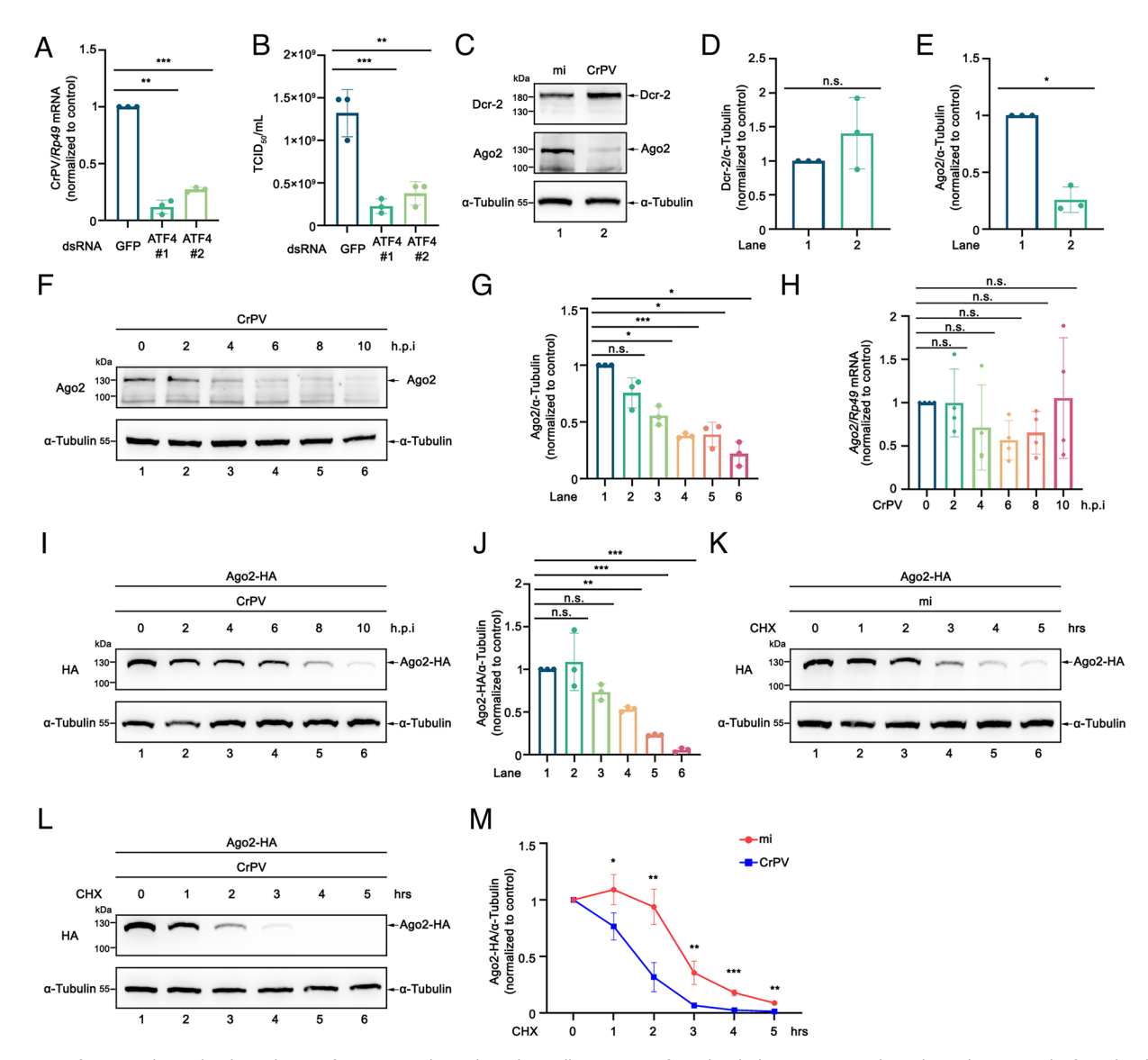


Fig. 3. CrPV infection induces the degradation of Ago2. (A and B) Cultured S2 cells were transfected with dsRNAs against the indicated genes and infected with CrPV (MOI = 1) for 12 h. The samples were subsequently analyzed by RT-qPCR to quantify CrPV genomic RNA levels (A) or by TCID<sub>50</sub> assay to measure viral titers (B). (C) Cultured S2 cells were mock infected or infected with CrPV (MOI = 1) for 12 h and subjected to western blot analysis using indicated antibodies. (D and E) Quantification of relative Dcr-2 (D) or Ago2 (E) levels in (C) from three independent experiments. (F) Cultured S2 cells were infected with CrPV (MOI = 1) for 0, 2, 4, 6, 8, or 10 h and then subjected to western blot analysis using indicated antibodies. (G) Quantification of relative Ago2 levels in (F) from three independent experiments. (H) Cultured S2 cells were infected with CrPV (MOI = 1) for 0, 2, 4, 6, 8, or 10 h and then analyzed by RT-qPCR to quantify Ago2 mRNA levels. (I) Cultured S2 cells were transfected with plasmid expressing Ago2-HA and then infected with CrPV (MOI = 1) for 0, 2, 4, 6, 8, or 10 h. Cell lysates were subsequently subjected to western blot analysis using indicated antibodies. (/) Quantification of relative Ago2-HA levels in (/) from three independent experiments. (K and L) Cultured S2 cells were transfected with plasmid expressing Ago2-HA and then mock infected (K) or infected with CrPV (MOI = 1) (L) for 4 h. After that, cells were treated with CHX for the indicated periods. Cell lysates were subsequently subjected to western blots using indicated antibodies. (M) Quantification of relative Ago2-HA levels in (K and L) from three independent experiments.

The siRNA pathway is the major antiviral pathway for (+) ssRNA (single-stranded positive-sense RNA) viruses in *Drosophila*. Dcr-2 and Ago2 are two core components of the Drosophila siRNA pathway (46–48) and are essential for the RNAi-mediated antiviral response (11–14). Our western blot analysis revealed that Ago2, but not Dcr-2, was significantly reduced during CrPV infection (Fig. 3C; quantified in Fig. 3 D and E), which is consistent with a previous study (49). In addition, we observed a significant decrease in Ago2 protein level at 4 h post CrPV infection (Fig. 3F; quantified in Fig. 3G), which aligns with the time point at which CrPV triggered an increase in P-eIF2α (Fig. 1 C and D). In contrast, the transcription level of Ago2 did not significantly decrease (Fig. 3H). Next, we ectopically expressed Ago2 with a C-terminal HA tag (Ago2-HA) in S2 cells. CrPV infection dramatically decreased ectopically expressed Ago2 (Fig. 31;

quantified in Fig. 3J) but did not affect ectopically expressed GFP (SI Appendix, Fig. S14A; quantified in SI Appendix, Fig. S14B). Moreover, we assessed the degradation rate of Ago2-HA by using the protein synthesis inhibitor cycloheximide (CHX). Compared to mock infection, CrPV infection significantly increased the degradation rate of Ago2 (Fig. 3 K and L, quantified in Fig. 3M). These results indicated that CrPV infection primarily reduces Ago2 by promoting its degradation.

We next sought to determine whether the ISR is involved in the process of Ago2 degradation. Induction of the ISR by knocking down ppp1r15 or Heat shock protein 70 cognate 3 (Hsc70-3), a key repressor of the PERK-phospho-eIF2α-ATF4 pathway, significantly decreased the protein level of Ago2-HA in S2 cells (Fig. 4 A and C; quantified in Fig. 4 B and D; knockdown efficiency validated in SI Appendix, Fig. S15 A and B). Similarly,

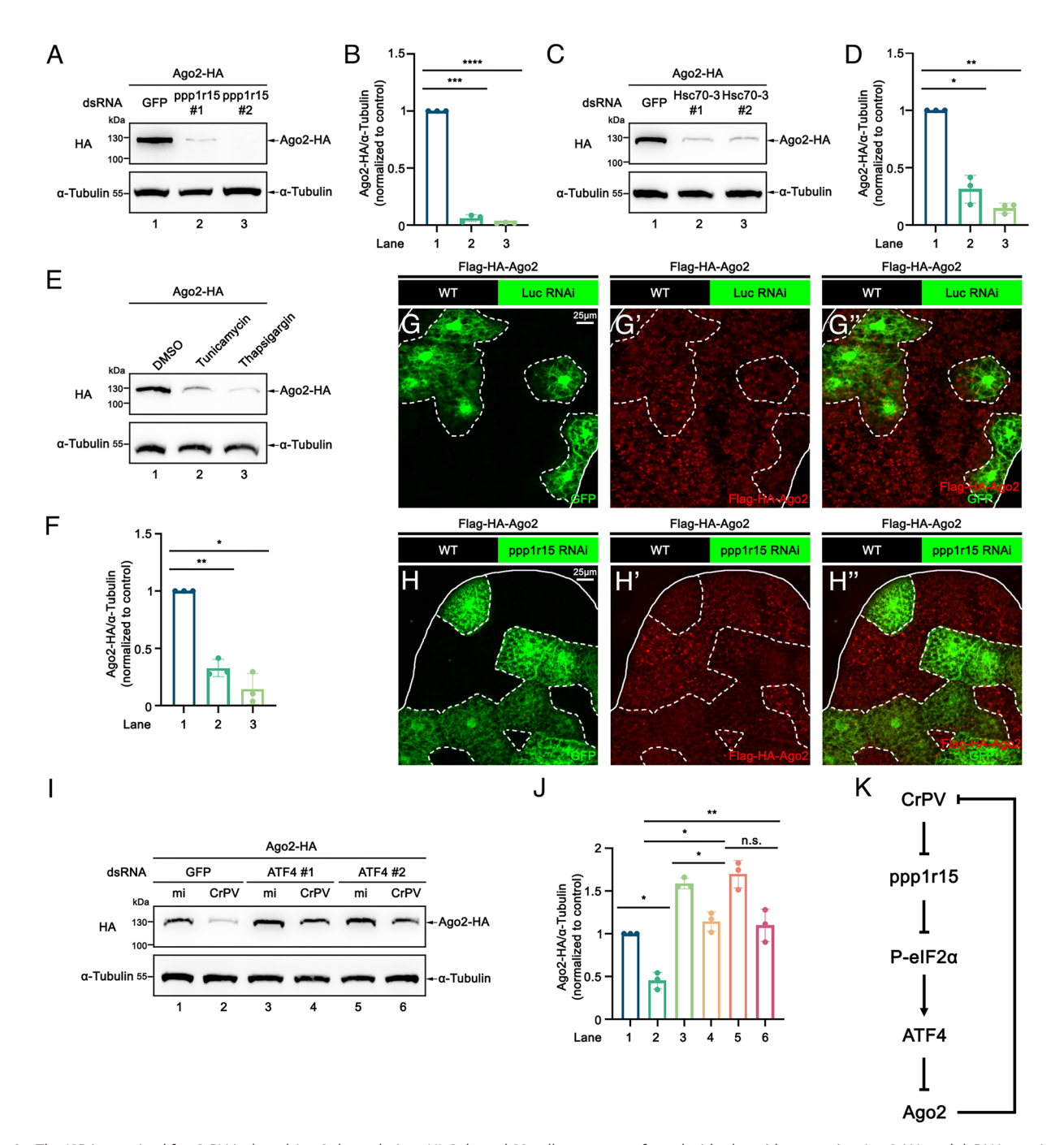


Fig. 4. The ISR is required for CrPV-induced Ago2 degradation. (A) Cultured S2 cells were transfected with plasmid expressing Ago2-HA and dsRNAs against the indicated genes. Cell lysates were subsequently subjected to western blot analysis using indicated antibodies. (B) Quantification of relative Ago2-HA levels in (A) from three independent experiments. (C) Cultured S2 cells were transfected with plasmid expressing Ago2-HA and dsRNAs against the indicated genes. Cell lysates were subsequently subjected to western blot analysis using indicated antibodies. (D) Quantification of relative Ago2-HA levels in (C) from three independent experiments. (E) Cultured S2 cells were transfected with plasmid expressing Ago2-HA for 36 h and then treated with DMSO, Tunicamycin, or Thapsigargin for 12 h. Cell lysates were subsequently subjected to western blot analysis using indicated antibodies. (F) Quantification of relative Ago2-HA levels in (F) from three independent experiments. (G and H) Fat bodies bearing GFP-labeled clones of indicated genotypes stained with anti-HA antibody (G' and H'). Merged images are shown in G" and H". (I) Cultured S2 cells were transfected with plasmid expressing Ago2-HA and dsRNAs against the indicated genes, and then mock infected or infected with CrPV (MOI = 1) for 12 h. Cell lysates were subsequently subjected to western blot analysis using indicated antibodies. (/) Quantification of relative Ago2-HA levels in (I) from three independent experiments. (K) Schematic diagram of CrPV infection induces the ISR to promote Ago2 degradation.

induction of the ISR by tunicamycin or thapsigargin, both of which are well-established PERK activators, also significantly decreased the protein level of Ago2-HA (Fig. 4E; quantified in Fig. 4F). Consistently, inducing of the ISR by knocking down ppp1r15 also decreased the protein level of Flag-HA-Ago2 in larval fat bodies (Fig. 4 G and H). Furthermore, inhibiting the ISR via ATF4 knockdown rescued CrPV-induced Ago2-HA degradation (Fig. 41; quantified in Fig. 41; knockdown efficiency validated in

SI Appendix, Fig. S15C). Taken together, our results demonstrated that the ISR promotes Ago2 degradation and thus suppresses antiviral RNAi response (Fig. 4K).

The ISR Promotes Ago2 Degradation By the Autophagy-Lysosomal Pathway. As we have found that CrPV induces the ISR to promote Ago2 degradation, we sought to investigate which protein degradation pathway(s) are involved in this process. Because the proteasome pathway and autophagy-lysosomal pathway are two major protein degradation pathways, we treated S2 cells with proteasome pathway inhibitor MG-132 or autophagy-lysosomal pathway inhibitor Bafilomycin A1. The results showed that, during viral infection, the Ago2 protein levels could be restored by Bafilomycin A1 but not MG-132 (Fig. 5A; quantified in Fig. 5B), indicating that the autophagy-lysosomal pathway is involved in CrPV-induced degradation of Ago2. Interestingly, ectopically expressed Ago2-HA was dramatically rescued by both inhibitors (Fig. 5C; quantified in Fig. 5D), which is consistent with previous study that ectopically expressed Ago2-HA degradation is mediated by the CrPV-1A/Cul2-Rbx1-EloBC ubiquitin E3 ligase complex (49). The reason for this contradictory observation may be that the proteasome pathway contributes only to the degradation of overly expressed Ago2 without affecting the basal level of Ago2.

Autophagy-related 8 (Atg8)/microtubule associated protein 1 light chain 3 (LC3) has been identified as a central player in the autophagy-lysosomal pathway through its interaction with cargo-bound receptors (50). We next investigated whether Ago2 forms a complex with Atg8a, the Drosophila homolog of mammalian Atg8/LC3. Our data showed that Ago2 was coprecipitated with Atg8a in S2 cells (Fig. 5 E and F) and colocalized with mCherry-Atg8a-positive autophagosomes after starvation-induced autophagy in larval fat bodies (Fig. 5 *G* and *H*). In order to confirm the CrPV infection indeed triggers the autophagy-lysosomal pathway, we assessed the protein level of refractory to sigma P (Ref(2) P), the Drosophila homolog of mammalian p62 and a specific substrate for the autophagy-lysosomal protein degradation pathway. As anticipated, our data showed that Ref(2)P degradation corresponded to the progression of CrPV infection (Fig. 51; quantified in Fig. 51) and this degradation process required ATF4 (Fig. 5K; quantified in Fig. 5*L*; knockdown efficiency validated in *SI Appendix*, Fig. S16*A*). Next, we attempted to determine whether the ISR is sufficient to trigger the autophagy-lysosomal pathway. We found that the protein level of Ref(2)P was significantly reduced in the context of ppp1r15 knockdown (Fig. 5M; quantified in Fig. 5N; knockdown efficiency validated in SI Appendix, Fig. S16B). Consistently, inducing the ISR by knocking down ppp1r15 increased the number of autophagosomes (Fig. 5 O-R) and lysosomes (SI Appendix, Fig. S17 A-D) in larval fat bodies and wing discs. Altogether, our findings revealed that the ISR promotes the autophagy-lysosomal pathway to degrade Ago2.

The ISR Promotes the Autophagy-Lysosomal Pathway by Up-Regulating Autophagy-Related Genes. We next investigated how the ISR promotes the autophagy-lysosomal pathway in *Drosophila*. To this end, we conducted a transcriptomic analysis to identify genes regulated by the knockdown of ppp1r15 in S2 cells. The transcriptomic analysis revealed a substantial number of differential expression genes (DEGs) regulated by the ISR (Fig. 6 A and B, differential expression of RNA-seq data shown in SI Appendix, Tables S1 and S2). Our Venn diagrams showed that there were 1,110 up-regulated genes and 705 down-regulated genes in both two ppp1r15 knockdown groups (Fig. 6 C and D, detailed data shown in SI Appendix, Tables S3 and S4). Given that Ago2 degradation is regulated by the autophagy-lysosomal pathway, we analyzed the expression levels of genes included in the autophagy-animal pathway of the Kyoto Encyclopedia of Genes and Genomes (KEGG) database (SI Appendix, Fig. S18A; transcripts per million (TPMs) data shown in SI Appendix, Table S5; ppp1r15 TPMs shown in SI Appendix, Fig. S18B). Notably, Autophagy-related 12 (Atg12), similar (sima), Atg8a, Atg1, PERK, and Inositol-requiring enzyme-1 (Ire1) were up-regulated upon ppp1r15 knockdown (SI Appendix, Fig. S18C; detailed data shown in SI Appendix, Table S6; heatmap shown in

Fig. 6E). These results were further confirmed by RT-qPCR (Fig. 6 F-K; knockdown efficiency validated in SI Appendix, Fig. S19A). Moreover, ATF4 knockdown significantly attenuated Atg1 transcription induced by ppp1r15 knockdown, while moderately suppressing ppp1r15 knockdown-mediated up-regulation of Atg8a, PERK, and Ire1 (Fig. 6 L-Q; knockdown efficiency validated in SI Appendix, Fig. S19 B and C). Similarly, CrPV infection promoted Atg1 transcription (Fig. 6R), but not that of other tested genes (SI Appendix, Fig. S20 A–E). This pattern is not fully consistent with the transcriptional upregulation induced by ppp1r15 knockdown, possibly due to CrPV activating other undefined signaling pathways. Interestingly, a previous study has demonstrated that overexpression of Atg1, the Drosophila homolog of the mammalian unc-51-like kinase 1 (ULK1), is sufficient to induce high level of autophagy in Drosophila (51). Based on this, we investigated whether ectopic expression of Atg1 is sufficient to induce the degradation of Ago2. We found that ectopic expression of Atg1 significantly reduced Ago2 protein level in S2 cells (Fig. 6S, quantified in Fig. 6T). Taken together, our results demonstrated that the ISR up-regulates Atg1 transcription in an ATF4-dependent manner, and this process is sufficient to promote Ago2 degradation via the autophagy-lysosomal pathway (Fig. 6U).

The ISR Promotes the Degradation of Other Ago2-RISC Components. Ago2 is a core component of the Ago2-RISC, which consists of Ago2, Fragile X messenger ribonucleoprotein 1 (FMR1), RM62, and Vasa intronic gene (VIG). This multiprotein complex plays a pivotal role in mediating siRNA-directed RNA degradation, a fundamental process in RNAi-based antiviral defense. We next investigated whether other components of Ago2-RISC are also degraded by the ISR-induced autophagy-lysosomal pathway. To this end, we respectively transfected S2 cells with HA-tagged FMR1 (FMR1-HA), RM62 (RM62-HA), and VIG (HA-VIG). Our western blots analysis revealed that the protein levels of these components were markedly decreased in conjunction with the progression of CrPV infection (Fig. 7 A, C, and E; quantified in Fig. 7 B, D, and F). Notably, induction of the ISR through ppp1r15 knockdown also led to a significant decrease in the protein levels of these RISC components (Fig. 7 G, I, and K; quantified in Fig. 7 H, J, and L; knockdown efficiency validated in SI Appendix, Fig. S21 *A*–*C*). Importantly, the CrPV-mediated depletion of FMR1, RM62, and VIG was effectively reversed upon treatment with the autophagy inhibitor Bafilomycin A1 (Fig. 7 M, O, and Q; quantified in Fig. 7 N, P, and R). Consistently, coimmunoprecipitation assays confirmed the interaction of FMR1, RM62, and VIG with Atg8a (Fig. 7 S-X). Moreover, ectopic expression of Atg1 substantially reduced the protein levels of these RISC components (Fig. 7 Y, AA, and AC, quantified in Fig. 7 Z, AB and AD).

It remains unclear whether CrPV-induced autophagy selectively targets the intact RISC or degrades individual components independently. To this end, we knocked down distinct RISC components and tested whether CrPV-mediated degradation of other RISC components were affected. Our data showed that knockdown of FMR1, RM62, or VIG did not rescue CrPV-induced Ago2 degradation (SI Appendix, Fig. S22 A, D and G, quantified in SI Appendix, Fig. S22 B, E and H; knockdown efficiency validated in SI Appendix, Fig. S22 C, F and I), demonstrating that CrPV-induced Ago2 degradation occurs independently of these RISC components. Conversely, Ago2 knockdown rescued CrPVinduced degradation of RM62 and VIG (SI Appendix, Fig. S22 M and P, quantified in SI Appendix, Fig. S22 N and Q; knockdown efficiency validated in SI Appendix, Fig. S22 O and R) but not FMR1 (SI Appendix, Fig. S22J, quantified in SI Appendix, Fig. S22K; knockdown efficiency validated in SI Appendix, Fig. S22L), indicating that

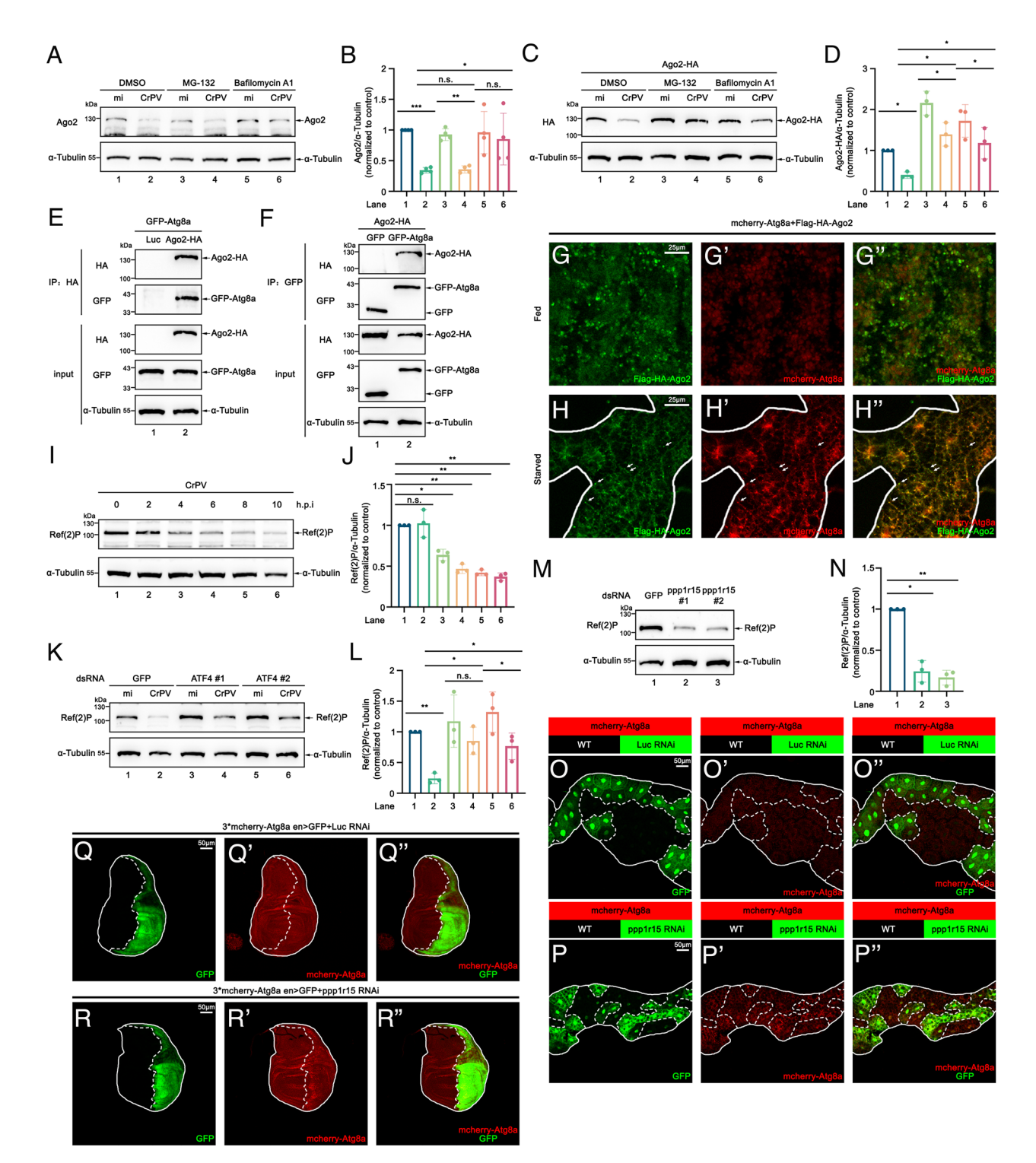


Fig. 5. CrPV infection and the ISR induce Ago2 degradation via the autophagy-lysosomal pathway. (A) Cultured S2 cells were mock infected or infected with CrPV (MOI = 1) and treated with DMSO, MG-132, or Bafilomycin A1 for 12 h. Cell lysates were subsequently subjected to western blot analysis using indicated antibodies. (B) Quantification of relative Ago2 levels in (A) from four independent experiments. (C) Cultured S2 cells were transfected with plasmid expressing Ago2-HA for 36 h and then mock infected or infected with CrPV (MOI = 1) and treated with DMSO, MG-132, or Bafilomycin A1 for 12 h. Cell lysates were subsequently subjected to western blot analysis using indicated antibodies. (D) Quantification of relative Ago2-HA levels in (C) from three independent experiments. (E and F) Cultured S2 cells were transfected with plasmids expressing the indicated proteins. Cell lysates were prepared and subjected to co-IP using anti-HA antibody (E) or anti-GFP antibody (F). Immunoprecipitates and total cell lysates (input) were subsequently subjected to western blot analysis using indicated antibodies. (G and H) Fat bodies from flies of indicated genotypes, either fed (G) or starved (H) for 8 h prior to dissection, were stained with anti-HA antibody. mCherry-Atg8a-positive autophagosomes are shown in G' and H'. Merged images are shown in G" and H". (I) Cultured S2 cells were infected with CrPV (MOI = 1) for 0, 2, 4, 6, 8, or 10 h and then subjected to western blot analysis using indicated antibodies. (/) Quantification of relative Ref(2)P levels in (/) from three independent experiments. (K) Cultured S2 cells were transfected with dsRNAs against the indicated genes and then mock infected or infected with CrPV (MOI = 1) for 12 h. Cell lysates were subsequently subjected to western blot analysis using indicated antibodies. (L) Quantification of relative Ref(2)P levels in (K) from three independent experiments. (M) Cultured S2 cells were transfected with dsRNAs against the indicated genes and subjected to western blot analysis using indicated antibodies. (N) Quantification of relative Ref(2)P levels in (M) from three independent experiments. (O and P) Fat bodies bearing GFP-labeled clones of indicated genotypes. mCherry-Atg8a-positive autophagosomes are shown in O' and P'. Merged images are shown in O" and P". (Q and R) Wing discs from flies of indicated genotypes. mCherry-Atg8a-positive autophagosomes are shown in Q' and R'. Merged images are shown in Q" and R".

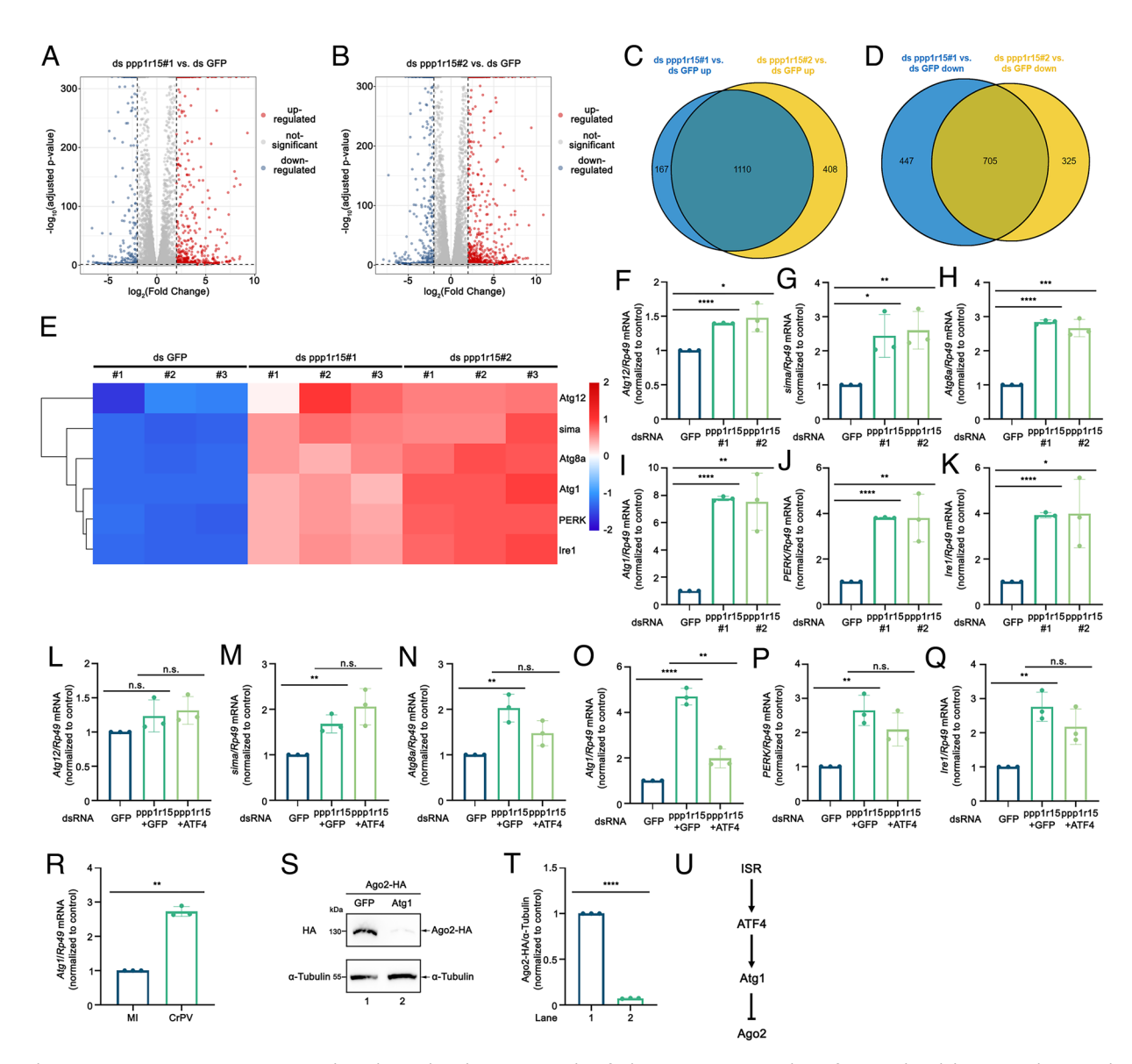


Fig. 6. The ISR promotes Atg1 transcription. (A and B) Volcano plots showing DEGs identified in transcriptomic analysis of ppp1r15 knockdown. (C and D) Venn diagrams showing up-regulated (C) and down-regulated (D) genes common to both ppp1r15 knockdown groups. (E) Heatmap depicting transcriptional changes in selected genes across ppp1r15 knockdown groups and the control group. (F-Q) S2 cells were transfected with dsRNAs against the indicated genes and analyzed by RT-qPCR to quantify mRNA levels of indicated genes. (R) Cultured S2 cells were mock infected or infected with CrPV (MOI = 1) for 6 h and then analyzed by RT-qPCR to quantify Atg1 mRNA levels. (5) Cultured S2 cells were transfected with plasmids expressing the indicated proteins and then subjected to western blot analysis using indicated antibodies. (7) Quantification of relative Ago2-HA levels in (5) from three independent experiments. (U) Schematic diagram of the ISR promotes Atg1 transcription

RM62 and VIG degradation require Ago2 while FMR1 degradation occurs through an Ago2-independent mechanism. These results suggested that while the intact RISC is not required for CrPV-mediated Ago2 degradation, the degradation of RISC components RM62 and VIG is Ago2-dependent, whereas FMR1 degradation appears to operate through a distinct mechanism. Taken together, our findings demonstrated that the ISR promotes the degradation of multiple Ago2-RISC components via the autophagy-lysosomal pathway, highlighting a broader regulatory mechanism that modulates the RNAi machinery during viral infection and stress responses.

### **Discussion**

The siRNA pathway serves as a potent antiviral defense mechanism in both vertebrates and invertebrates. In the present study, we uncover an unexpected crosstalk between the ISR and siRNA pathways. Our data show that inhibiting the PP1 subunit ppp1r15 is sufficient to lead to the degradation of Ago2-RISC components, thereby suppressing the siRNA pathway. Transcriptomic analysis enables us to identify Atg1 as a downstream transcription product of the phospho-eIF2α-ATF4 signaling axis. Atg1 emerges as a principal regulatory factor mediating the degradation of Ago2 through the autophagy-lysosomal pathway, thus further suppressing the antiviral RNAi response (SI Appendix, Fig. S23). Collectively, our findings reveal a previously undescribed upstream regulatory mechanism of the siRNA pathway, which is utilized by CrPV to evade antiviral RNAi response.

The ISR is triggered in eukaryotic cells by various stress stimulus, including hypoxia, nutrient deprivation, oncogene activation, heme deficiency, ultraviolet light, reactive oxygen species (ROS), endoplasmic reticulum (ER) stress, and viral infection (52–63). Based on our finding that the ISR can suppress the RNAi pathway, we propose that other upstream stressors, in addition to the viral infection described in this paper, that activate the ISR may also suppress RNAi responses and consequently weaken antiviral immunity. On the other hand, the ISR is mainly mediated

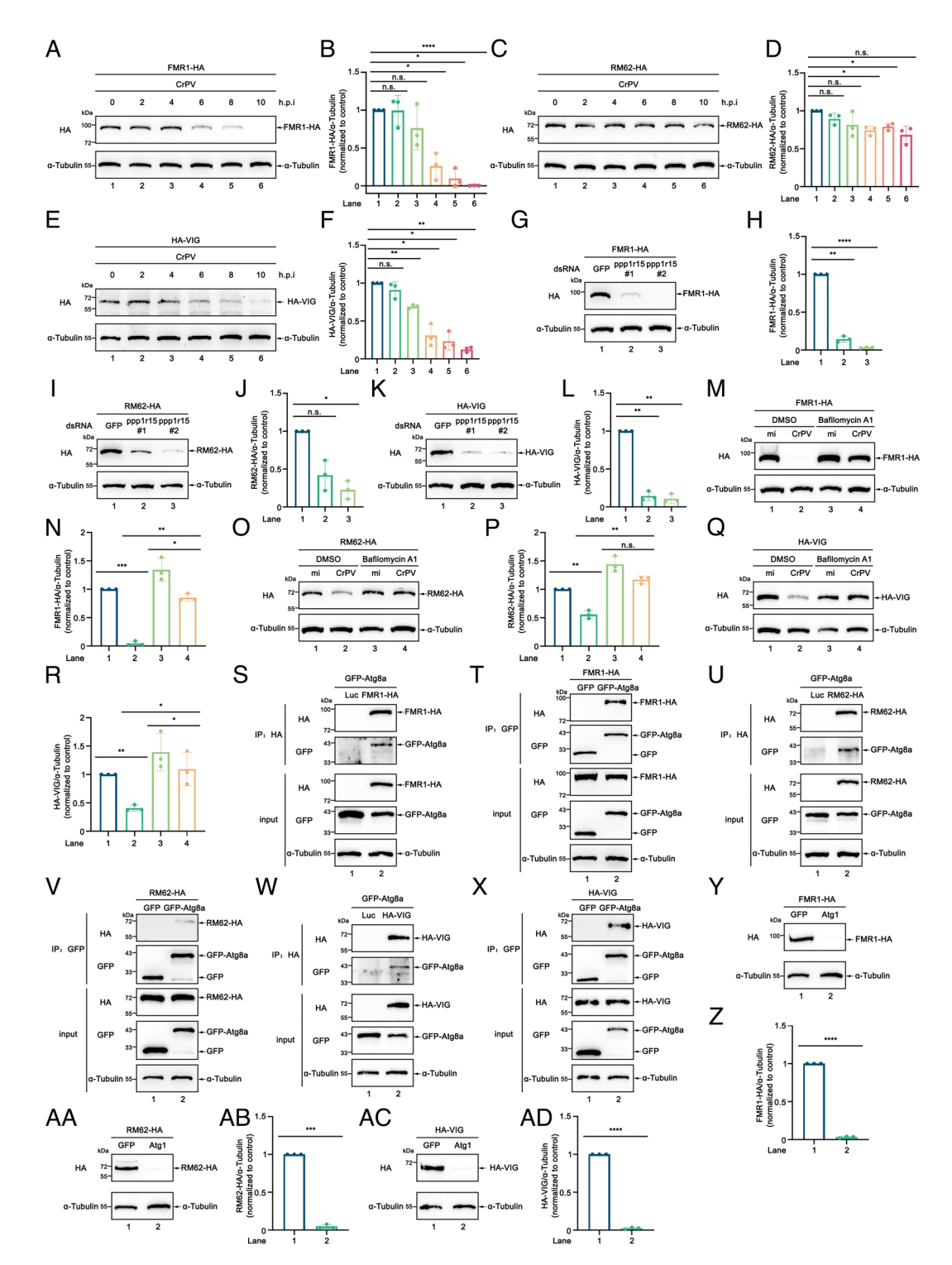


**Fig. 7.** CrPV infection and the ISR promote the degradation of Ago2-RISC components. (*A*, *C*, and *E*) Cultured S2 cells were transfected with plasmid expressing FMR1-HA (*A*), RM62-HA (*C*), or HA-VIG (*E*) and then infected with CrPV (MOI = 1) for 0, 2, 4, 6, 8, or 10 h. Cell lysates were subsequently subjected to western blot analysis using indicated antibodies. (*B*, *D*, and *P*) Quantification of relative FMR1-HA (*B*), RM62-HA (*D*), and HA-VIG (*F*) levels in (*A*, *C*, and *E*) from three independent experiments. (*G*, *I*, and *K*) Cultured S2 cells were transfected with plasmid expressing FMR1-HA (*B*), RM62-HA (*D*), or HA-VIG (*K*) and dsRNAs against the indicated genes. Cell lysates were subsequently subjected to western blot analysis using indicated antibodies. (*H*, *J*, and *L*) Quantification of relative FMR1-HA (*H*), RM62-HA (*D*), and HA-VIG (*L*) levels in (*G*, *I*, and *K*) from three independent experiments. (*M*, *O*, and *Q*) Cultured S2 cells were transfected with plasmid expressing FMR1-HA (*M*), RM62-HA (*D*), and HA-VIG (*C*) for 36 h and then mock infected or infected with CrPV (MOI = 1) and treated with DMSO or Bafilomycin A1 for 12 h. Cell lysates were subsequently subjected to western blot analysis using indicated antibodies. (*N*, *P*, and *R*) Quantification of relative FMR1-HA (*N*), RM62-HA (*P*), and HA-VIG (*R*) levels in (*M*, *O*, and *Q*) from three independent experiments. (*S*-X) Cultured S2 cells were transfected with plasmids expressing the indicated proteins. Cell lysates were prepared and subjected to co-IP using anti-HA antibody (*S*, *U*, and *W*) or anti-GFP antibody (*T*, *V*, and *X*). Immunoprecipitates and total cell lysates (input) were subsequently subjected to western blot analysis using indicated antibodies. (*Y*, *AA*, and *AC*) Cultured S2 cells were transfected with plasmids expressing the indicated proteins and then subjected to western blot analysis using indicated antibodies. (*Z*, *B* and *AD*) Quantification of relative FMR1-HA (*Z*), RM62-

by the PERK and PKR in response to (+)ssRNA virus infections. In this study, we propose a mechanism through which (+)ssRNA viruses activate the ISR: by inhibiting the PP1 subunit ppp1r15,

which leads to the suppression of eIF2 $\alpha$  dephosphorylation, and, in turn, activates the ISR. This nonclassical mechanism of ISR activation may also apply to other RNA virus infections.

Our results indicated that ectopically expressed Ago2 can be targeted for degradation via both the ubiquitin—proteasome pathway and the autophagy-lysosomal pathway during CrPV infection (Fig. 5 C and D). These findings are consistent with the earlier study by Nayak et al., which demonstrated that CrPV-1A recruits Cul2-Rbx1-EloBC ubiquitin E3 ligase complex, thereby promoting the degradation of ectopically expressed Ago2 (49). Interestingly, this degradation mechanism did not apply to basal level Ago2 in the context of CrPV infection (Fig. 5 A and B). As a possible explanation, we suggest that in response to excessive amounts of Ago2, CrPV employs various mechanisms to degrade Ago2. Conversely, under conditions of normal Ago2 level, this virus predominantly utilizes the autophagy-lysosomal pathway to degrade Ago2. This variable mechanism may be used by CrPV to counteract antiviral RNAi responses in cells with different immune states.

Our data indicated that ISR can enhance CrPV replication (Fig. 3 A and B). In contrast, earlier findings showed that the ISR does not significantly influence CrPV production (35). This conclusion was based on observations that ectopically expressed ppp1r15 failed to inhibit host translation or CrPV production (35). We believe the discrepancies may arise from low plasmid transfection efficiency in S2 cells, which could lead to insufficient ectopic expression of ppp1r15 and thus failed to suppress CrPV production in their study. Furthermore, differences in methodology may also explain the conflicting results: while they measured viral protein synthesis, we assessed viral RNA and titer.

The differential impact of ISR on distinct RNA viruses presents intriguing implications. Our data demonstrated that ISR enhances DCV replication (SI Appendix, Fig. S10C; knockdown efficiency validated in SI Appendix, Fig. S10D) but does not significantly affect FHV (SI Appendix, Fig. S10A; knockdown efficiency validated in SI Appendix, Fig. S10B) or DXV (SI Appendix, Fig. S10E; knockdown efficiency validated in SI Appendix, Fig. S10F). As members of the Dicistroviridae family that utilize IRES-mediated translation, DCV and CrPV likely evade the detrimental effects of ISR-induced translational attenuation which primarily affects 5'-cap-dependent translation. This evasion enables them to exploit ISR-induced RNAi suppression for replicative advantage. Among dicistroviruses, CrPV activates ISR whereas DCV does not. This divergence may stem from distinct host adaptation strategies. CrPV infects diverse insect hosts including orthopteran, dipteran, and lepidopteran insects (64), while to our knowledge, DCV has only been found infecting dipteran insects under natural conditions. Compared to DCV, CrPV faces more complex host antiviral defenses across insect orders. We hypothesize that this pressure has driven CrPV to evolve distinct mechanisms, such as ISR induction, as a general strategy for infecting diverse hosts.

In summary, our study highlights the importance of virus-induced host stress responses in antiviral immunity and reveals the ISR as an upstream mechanism governing the antiviral siRNA pathway. Considering that the ISR can be triggered by various stress stimuli, activating this stress response could potentially regulate the intensity of antiviral responses, which has implications for pest management and insect population control. Furthermore, since both the ISR and the siRNA pathways are evolutionarily conserved across invertebrates and vertebrates, this may inspire further exploration of the innate immunity network in mammals and provide a theoretical foundation for the development of antiviral drugs.

### **Materials and Methods**

**Cell Culture and Transfection.** *Drosophila* S2 cell line (RRID: CVCL\_Z232) was obtained from the American Type Culture Collection (ATCC). Its identity was confirmed by visual inspection of the cell morphology in Schneider's *Drosophila* 

medium (Thermo Fisher Scientific, Cat #21720024)/10% fetal bovine serum (FBS). A *Mycoplasma* test is usually not done for S2 cells (65).

For transfection assay, S2 cells were plated in 100-mm plates or six-well plates and grown overnight to reach 70% confluence. After that, DNA plasmids or dsRNAs were transfected into the cells using FuGene HD transfection reagent (Promega, Cat #2311), following the manufacturer's protocol. In addition, while transfecting the same plasmid or dsRNA in multiple wells, to ensure equal transfection, cells cultured in a 100 mm plate were first transfected. After 24 to 42 h, the transfected cells were randomly divided into six-well plate, and cultured for an additional ~6 h to reach 70 to 80% confluence (approximately 2.5 \* 106 cells per well). The cells were then subjected to viral infection or other treatments according to experimental requirements.

**Fly Stocks.** All flies used were reared at 25 °C on a standard cornmeal/yeast diet. Fly strains used in this study are the following: hs-FLP; Sp/CyO; Act > CD2 > Gal4, UAS-GFP (BCF #658) and hs-FLP; Act > CD2 > Gal4, UAS-GFP; MKRS/TM6B (BCF #657) from Core Facility of Drosophila Resource and Technology (Center for Excellence in Molecular Cell Science, Chinese Academy of Sciences); UAS-Luciferase RNAi (BDSC #31603) and Flag-HA-Ago2 (BDSC #33242) from Bloomington *Drosophila* Stock Center; UAS-ppp1r15 RNAi (THU #1204) from Tsinghua fly center; en-Gal4, UAS-GFP, and 3\*mcherry-Atg8a from Dr. Tatsushi Igaki (Kyoto University, Kyoto, Japan); ppl-Gal4 and r4-mcherry-Atg8a from Dr. Sheng Li and Dr. Suning Liu (South China Normal University, Guangzhou, China). Detailed genotypes of fly strains used in this study are listed in *Sl Appendix*, Table S7.

**Viruses.** CrPV was kindly provided by Dr. Qingfa Wu (University of Science and Technology of China, Hefei, China). DCV was kindly provided by Dr. Bo Liu (Xiamen University, Xiamen, China). FHV and DXV were kindly provided by Dr. Liqing Zhang (Hangzhou Normal University, Hangzhou, China). The viral titers were determined using the 50% tissue culture infectious dose (TCID<sub>50</sub>).

**Dual-Luciferase Reporter Assay.** To construct the FLU and RLU reporter plasmids, the firefly luciferase or renilla luciferase ORF was cloned into the *EcoR I-Xho I* site of the pAc5.1/V5-His vector. For the *ATF4* 5'UTR-FLU reporter plasmid, the *ATF4* 5'UTR replaced the 5'UTR region of FLU reporter plasmid. To construct the FLU-CrPV IGR-RLU reporter plasmid, the firefly luciferase-CrPV IGR-renilla luciferase sequence was amplified from the pFR\_CrPV\_xb plasmid (Addgene, Cat #11509) and inserted into the *EcoR I-Xho I* site of the pAc5.1/V5-His vector. To construct the CrPV 5'IRES-FLU reporter plasmid, the CrPV 5'IRES replaced the 5'-UTR region of FLU reporter plasmid. Importantly, the methionine initiator codon of the firefly luciferase was deleted and replaced by the first 16 codons of the CrPV ORF1 protein, as described in a previous study (42). Dual-Luciferase reporter assay was performed using Dual-Luciferase® Reporter Assay System (Promega, Cat #E1910), following the manufacturer's protocol.

**Transcriptomic Sequencing and Analysis.** Total RNA was extracted from cells using the RNA isolater Total RNA Extraction Reagent (Vazyme, Cat #R401-01). The mRNA was then enriched and reverse-transcribed to construct a cDNA library. The cDNA libraries were sequenced using the Illumina NovaSeq 6000 (Illumina, San Diego, USA). mRNA enrichment, reverse transcription, cDNA library construction, quality control, and sequencing were performed by Biomarker Technologies (Biomarker Technologies Ltd, Beijing, China). The analysis of transcriptomic sequencing data was performed on the Secevo HPC cluster of the School of Ecology, Sun Yat-sen University (Shenzhen, China). DEGs were identified using DESeq2. DEGs with an absolute  $\log_2$  fold change ( $|\log_2$ FC|) $\geq$ 1 and adjusted P-value (padj)  $\leq$  0.05 were considered to be significantly DEGs. Heatmap and Venn diagram analyses were performed by using tools in Hiplot Pro (https://hiplot.com.cn/), a comprehensive web service for biomedical data analysis and visualization.

**Statistical Analysis.** Statistical significance was assessed using a Student's t test for comparisons between two groups and a one-way ANOVA multiple-comparison test for comparisons among multiple groups. In all figures, significance is indicated as follows: P > 0.05 (not significant, n.s.), \*P < 0.05, \*\*P < 0.01, \*\*\*P < 0.001, and \*\*\*\*P < 0.0001.

**Data, Materials, and Software Availability.** The RNA-seq data have been deposited in Gene Expression Omnibus (GSE309081) (66). All other study data are included in the article and/or *SI Appendix*.

ACKNOWLEDGMENTS. This study was supported by grants from the Fundamental Research Funds for the Central Universities, Sun Yat-sen University (Grant No. 22hytd05 to Z.W.), and the Major Project of Guangzhou National Laboratory (Grant No. GZNL2024A01017 to Z.W.). We thank Dr. Tatsushi Igaki (Kyoto University, Kyoto, Japan), Dr. Sheng Li and Dr. Suning Liu (South China Normal University, Guangzhou, China), Dr. Qingfa Wu (University of Science and Technology of China, Hefei, China), Dr. Bo Liu (Xiamen University, Xiamen, China), Dr. Liqing Zhang (Hangzhou Normal University, Hangzhou, China), the Bloomington Drosophila Stock Center, the FlyORF, the Tsinghua fly center, and the Core Facility of Drosophila Resource and Technology (Center for Excellence in Molecular Cell Science, Chinese Academy of Sciences) for viruses and fly stocks. We thank the computational resources provided by the Secevo HPC cluster at the School of Ecology, Sun Yatsen University (Shenzhen, China). We also thank Dr. Yuan Zou, Dr. Rongfeng Cui (Sun Yat-sen University, Shenzhen, China), and the members of the Wang laboratory for helpful discussions.

Author affiliations: aState Key Laboratory of Biocontrol, School of Ecology, Sun Yat-sen University, Shenzhen 518107, China

- J. A. Hoffmann, The immune response of Drosophila. Nature 426, 33-38 (2003).
- J. Xu, S. Cherry, Viruses and antiviral immunity in drosophila. Dev. Comp. Immunol. 42, 67-84
- C. Kemp & JL Imler Antiviral immunity in drosophila. Curr. Opin. Immunol. 21, 3-9 (2009).
- J. A. Hoffmann, F. C. Kafatos, C. A. Janeway, R. A. Ezekowitz, Phylogenetic perspectives in innate immunity. Science (New York, N.Y.), 284, 1313-1318 (1999).
- B. Lemaitre, J. Hoffmann, The host defense of Drosophila melanogaster. Annu. Rev. Immunol. 25, 697-743 (2007).
- J. Schneider, J. L. Imler, Sensing and signalling viral infection in drosophila. Dev. Comp. Immunol. **117**, 103985 (2021).
- R. A. Zambon, M. Nandakumar, V. N. Vakharia, L. P. Wu, The Toll pathway is important for an antiviral response in Drosophila. Proc. Natl. Acad. Sci. U.S.A. 102, 7257-7262 (2005).
- Á. G. Ferreira et al., The toll-dorsal pathway is required for resistance to viral oral infection in Drosophila. PLoS Pathog. 10, e1004507 (2014).
- A. Costa, E. Jan, P. Sarnow, D. Schneider, The IMD pathway is involved in antiviral immune responses in Drosophila. PLoS One 4, e7436 (2009).
- V. Avadhanula, B. P. Weasner, G. G. Hardy, J. P. Kumar, R. W. Hardy, A novel system for the launch of alphavirus RNA synthesis reveals a role for the Imd pathway in arthropod antiviral response. PLoS Pathog. 5, e1000582 (2009).
- H. Li, W. X. Li, S. W. Ding, Induction and suppression of RNA silencing by an animal virus. Science (New York, N.Y.), 296, 1319-1321 (2002)
- D. Galiana-Arnoux, C. Dostert, A. Schneemann, J. A. Hoffmann, & Imler JL Essential function in vivo for Dicer-2 in host defense against RNA viruses in drosophila. Nature Immunol. 7, 590-597 (2006).
- S. Mueller et al., RNAi-mediated immunity provides strong protection against the negative-strand RNA vesicular stomatitis virus in *Drosophila*. Proc. Natl. Acad. Sci. U.S.A. **107**, 19390-19395 (2010).
- X. H. Wang et al., RNA interference directs innate immunity against viruses in adult Drosophila. Science (New York, N.Y.), 312, 452-454 (2006).
- Y. Qiu et al., Flavivirus induces and antagonizes antiviral RNA interference in both mammals and mosquitoes. Sci. Adv. 6, eaax7989 (2020).
- Y. Qiu et al., Human virus-derived small RNAs can confer antiviral immunity in mammals. Immunity 46, 992-1004.e1005 (2017).
- Y. Li et al., Induction and suppression of antiviral RNA interference by influenza A virus in mammalian cells. Nature Microbiol. 2, 16250 (2016).
- Y. Li, J. Lu, Y. Han, X. Fan, S. W. Ding, RNA interference functions as an antiviral immunity mechanism in mammals. Science (New York, N.Y.), 342, 231-234 (2013).
- P. V. Maillard et al., Antiviral RNA interference in mammalian cells. Science (New York, N.Y.), 342, 235-238 (2013).
- J. Kong et al., Alphavirus infection triggers antiviral RNAi immunity in mammals. Cell Rep. 42, 112441 (2023).
- 21. D. S. Schwarz et al., Asymmetry in the assembly of the RNAi enzyme complex. Cell 115, 199-208 (2003).
- 22. Q. Liu et al., R2D2, a bridge between the initiation and effector steps of the Drosophila RNAi pathway. Science (New York, N.Y.), 301, 1921-1925 (2003).
- J. T. Marques et al., Loqs and R2D2 act sequentially in the siRNA pathway in Drosophila. Nat. Struct. Mol. Biol. 17, 24-30 (2010).
- R. P. van Rij et al., The RNA silencing endonuclease Argonaute 2 mediates specific antiviral immunity in Drosophila melanogaster. Genes Dev. 20, 2985-2995 (2006).
- S. Deddouche et al., The dexd/h-box helicase Dicer-2 mediates the induction of antiviral activity in drosophila. Nat. Immunol. 9, 1425-1432 (2008).
- Z. Wang et al., Drosophila dicer-2 has an RNA interference-independent function that modulates toll immune signaling. Sci. Adv. 1, e1500228 (2015).
- N. Donnelly, A. M. Gorman, S. Gupta, A. Samali, The elF2 $\alpha$  kinases: their structures and functions. Cellular Mol. Sci.: CMLS 70, 3493-3511 (2013).
- Y. Wu, Z. Zhang, Y. Li, Y. Li, The regulation of integrated stress response signaling pathway on viral infection and viral antagonism. *Front. Microbiol.* **12**, 814635 (2021).
- S. B. Lee et al., The interferon-induced double-stranded RNA-activated human p68 protein kinase potently inhibits protein synthesis in cultured cells. Virology 192, 380-385 (1993).
- S. Balachandran et al., Essential role for the dsRNA-dependent protein kinase PKR in innate immunity to viral infection. Immunity 13, 129-141 (2000).
- $\hbox{D. F. Stojdl}\ \emph{et al.}, \hbox{The murine double-stranded RNA-dependent protein kinase PKR is required for a constant of the protein kinase pkg is a supplementation of the pkg$ resistance to vesicular stomatitis virus. J. Virol. 74, 9580-9585 (2000).
- M. Xue et al., The PERK arm of the unfolded protein response negatively regulates transmissible gastroenteritis virus replication by suppressing protein translation and promoting type I interferon production. J. Virol. 92, e00431-18 (2018).
- A. Jaspart et al., GCN2 phosphorylates HIV-1 integrase and decreases HIV-1 replication by limiting viral integration. Sci. Rep. 7, 2283 (2017).

- 34. J. Pino et al., GCN2 has inhibitory effect on human immunodeficiency virus-1 protein synthesis and is cleaved upon viral infection. PLoS One 7, e47272 (2012).
- J. L. Garrey, Y. Y. Lee, H. H. Au, M. Bushell, E. Jan, Host and viral translational mechanisms during cricket paralysis virus infection. J. Virol. 84, 1124-1138 (2010).
- A. Khong et al., Temporal regulation of distinct internal ribosome entry sites of the Dicistroviridae cricket paralysis virus. Viruses 8, 25 (2016).
- I. Novoa, H. Zeng, H. P. Harding, D. Ron, Feedback inhibition of the unfolded protein response by GADD34-mediated dephosphorylation of eIF2alpha. J. Cell Biol. 153, 1011-1022 (2001).
- D. Vasudevan et al., The GCN2-ATF4 signaling pathway induces 4E-BP to bias translation and boost antimicrobial peptide synthesis in response to bacterial infection. *Cell Rep.* **21**, 2039-2047 (2017). M. J. Kang *et al.*, 4E-BP is a target of the GCN2-ATF4 pathway during Drosophila development and
- aging. J. Cell Biol. 216, 115-129 (2017).
- E. Jan & Sarnow P., Factorless ribosome assembly on the internal ribosome entry site of cricket paralysis virus. *J. Mol. Biol.* **324**, 889–902 (2002).
- J. E. Wilson, M. J. Powell, S. E. Hoover, P. Sarnow, Naturally occurring dicistronic cricket paralysis virus RNA is regulated by two internal ribosome entry sites. Mol. Cell. Biol. 20, 4990-4999 (2000).
- K. Majzoub et al., RACK1 controls IRES-mediated translation of viruses. Cell 159, 1086-1095
- H. Y. Jiang, R. C. Wek, GCN2 phosphorylation of elF2alpha activates NF-kappaB in response to UV irradiation. Biochem. J. 385, 371-380 (2005).
- C. Dostert et al., The Jak-STAT signaling pathway is required but not sufficient for the antiviral response of drosophila. Nature Immunol. 6, 946-953 (2005).
- R. Shen et al., A dRASSF-STRIPAK-Imd-JAK/STAT axis controls antiviral immune response in Drosophila. Cell Rep. 40, 111143 (2022).
- y. S. Lee *et al.*, Distinct roles for *Drosophila* Dicer-1 and Dicer-2 in the siRNA/miRNA silencing pathways. *Cell* **117**, 69-81 (2004).
- K. Okamura, A. Ishizuka, H. Siomi, M. C. Siomi, Distinct roles for Argonaute proteins in small RNAdirected RNA cleavage pathways. Genes Dev. 18, 1655-1666 (2004).
- Y. Tomari, C. Matranga, B. Haley, N. Martinez, P. D. Zamore, A protein sensor for siRNA asymmetry. Science (New York, N.Y.), 306, 1377-1380. (2004).
- A. Nayak et al., A viral protein restricts Drosophila RNAi immunity by regulating argonaute activity and stability. Cell Host Microbe 24, 542-557, e549 (2018).
- T. Johansen, Lamark T., Selective Autophagy: ATG8 Family Proteins, LIR Motifs and Cargo Receptors. J. Mol. Biol. 432, 80-103 (2020).
- R. C. Scott, G. Juhász, T. P. Neufeld, Direct induction of autophagy by Atg1 inhibits cell growth and induces apoptotic cell death. Curr. Biol.: CB 17, 1-11 (2007).
- K. Pakos-Zebrucka et al., The integrated stress response. EMBO Rep. 17, 1374-1395 (2016).
- H. P. Harding et al., An integrated stress response regulates amino acid metabolism and resistance to oxidative stress. Mol. Cell 11, 619-633 (2003).
- T. E. Dever et al., Phosphorylation of initiation factor 2 alpha by protein kinase GCN2 mediates gene-specific translational control of GCN4 in yeast. *Cell* 68, 585–596 (1992).
- T. Rzymski et al., Regulation of autophagy by ATF4 in response to severe hypoxia. Oncogene 29, 4424-4435 (2010).
- J. Ye et al., The GCN2-ATF4 pathway is critical for tumour cell survival and proliferation in response 56. to nutrient deprivation. EMBO J. 29, 2082-2096 (2010).
- M. A. García, E. F. Meurs, M. Esteban, The dsRNA protein kinase PKR: Virus and cell control. Biochimie 89, 799-811 (2007).
- 58. H. P. Harding, Y. Zhang, & Ron D Protein translation and folding are coupled by an endoplasmicreticulum-resident kinase. Nature 397, 271-274 (1999).
- C. Denoyelle et al., Anti-oncogenic role of the endoplasmic reticulum differentially activated by mutations in the MAPK pathway. Nat. Cell Biol. 8, 1053-1063 (2006).
- L. S. Hart et al., ER stress-mediated autophagy promotes Myc-dependent transformation and tumor growth. J. Clin. Invest. 122, 4621-4634 (2012).
- H. J. Lu, N. Koju, & Sheng R Mammalian integrated stress responses in stressed organelles and their functions. Acta Pharmacol. Sin. 45, 1095-1114 (2024).
- J. Deng et al., Activation of GCN2 in UV-irradiated cells inhibits translation. Current Biol.: CB 12, 1279-1286 (2002).
- J. Han et al., ER-stress-induced transcriptional regulation increases protein synthesis leading to cell death. Nat. Cell Biol. 15, 481-490 (2013).
- C. Reinganum, The isolation of cricket paralysis virus from the emperor gum moth, Antheraea eucalypti Scott, and its infectivity towards a range of insect species. Intervirology 5, 97-102 (1975). N. Berndt et al., Ubiquitylation-independent activation of notch signalling by delta. eLife 6, e27346
- Q. Wang et al., The integrated stress response suppresses antiviral RNA interference by autophagymediated degradation of RNA-induced silencing complex. Gene Expression Omnibus. https://www. ncbi.nlm.nih.gov/geo/guery/acc.cgi?acc=GSE309081. Deposited 24 September 2025.